



Downscaling of real-time coastal flooding predictions for decision support

C. A. Rucker^{1,2} · N. Tull^{1,3} · J. C. Dietrich¹ · T. E. Langan⁴ · H. Mitasova⁵ · B. O. Blanton⁶ · J. G. Fleming⁷ · R. A. Luettich Jr⁸

Received: 27 July 2020 / Accepted: 10 February 2021

© The Author(s), under exclusive licence to Springer Nature B.V. part of Springer Nature 2021

Abstract

During coastal storms, forecasters and researchers use numerical models to predict the magnitude and extent of coastal flooding. These models must represent the large regions that may be affected by a storm, and thus, they can be computationally costly and may not use the highest geospatial resolution. However, predicted flood extents can be down-scaled (by increasing resolution) as a post-processing step. Existing downscaling methods use either a static extrapolation of the flooding as a flat surface, or rely on subsequent simulations with nested, full-physics models at higher resolution. This research explores a middle way, in which the downscaling includes simplified physics to improve accuracy. Using results from a state-of-the-art model, we downscale its flood predictions with three methods: (1) static, in which the water surface elevations are extrapolated horizontally until they intersect the ground surface; (2) slopes, in which the gradient of the water surface is used; and (3) head loss, which accounts for energy losses due to land cover characteristics. The downscaling methods are then evaluated for forecasts and hindcasts of Hurricane Florence (2018), which caused widespread flooding in North Carolina. The static and slopes methods tend to over-estimate the flood extents. However, the head loss method generates a downscaled flooding extent that is a close match to the predictions from a higher-resolution, full-physics model. These results are encouraging for the use of these downscaling methods to support decision-making during coastal storms.

Keywords ADCIRC · Carteret County · GRASS GIS · North Carolina · Storm Surge

1 Introduction

Tropical cyclones can be devastating to coastal communities. Katrina (2005) generated more than 10 m of combined wave action and surge along the Mississippi coast (Fritz et al. 2007), caused record-breaking damage and casualties in and near New Orleans, and led to major overhauls in hurricane protection planning and storm surge forecasting capabilities (Interagency Performance Evaluation Task Force 2008). Since Katrina, other storms

✉ J. C. Dietrich
jdietrich@ncsu.edu

Extended author information available on the last page of the article

have damaged the U.S. Gulf and Atlantic coasts, with the seven largest storms causing more than \$326 billion in damages (Smith et al. 2020). It is critical to predict the waves and surge associated with such powerful storms to support decision-makers (Cheung et al. 2003).

Numerical models can provide useful predictions of storm-driven flooding (e.g., Forbes et al. 2010; Blanton et al. 2012; Dietrich et al. 2013; Cyriac et al. 2018), typically by generating a map of the maximum water levels and the horizontal extents of flooding. These models must balance between accuracy (related to their temporal and spatial resolution) and efficiency (in terms of wall-clock time for the simulation). Accuracy is increased typically as the model resolution (or number of computational points) is increased, but this can also lead to a decrease in efficiency (Kerr et al. 2013). And, because numerical models must represent the large coastal regions that might be flooded during storms, they may not be able to represent efficiently the waves and surge at smaller scales. Resolution can be increased in specific regions of interest, but even state-of-the-art models for storm-driven coastal flooding have a typical resolution of 50 m or larger in overland regions, and thus cannot represent hazards at the scale of individual buildings or roadways. Those infrastructure components are of critical concern to emergency managers and other stakeholders, so there is a continuing need to extend flooding predictions to smaller, local scales, without sacrificing efficiency during storms.

Several studies have explored methods to represent flood risk at local scales, especially with the widespread availability of Light Detection and Ranging (LiDAR) and other surveys, which lead to high-accuracy Digital Elevation Models (DEMs) for the ground surface, and which typically have finer resolution than numerical models for the same region. Flooding predictions from the coarser-resolution numerical model can then be downscaled and extrapolated over the finer-resolution ground surface. This process has been implemented with two main approaches: *static* approaches use the so-called bathtub model to extend the flooding predictions as a flat surface over the topography, while *dynamic* approaches adjust the flooding predictions with nested models that enforce the mass and/or momentum conservation related to overland flooding.

In a static approach, all DEM cells are flooded where the input water level (say, from a predictive, full-physics model) is greater than the elevation of the ground surface in the DEM; hydraulic connection may or may not be considered. For studies of flood mapping and risk analysis under sea-level-rise scenarios, the system-wide flooding may occur over many years or decades, and thus a static approach may be suitable (Brown 2006; Poulter and Halpin 2008; Knowles 2010; Lichter and Felsenstein 2012; Heberger et al. 2009). For studies of flooding due to storm surge, the static approach may also be sufficient, depending on the spatial scales of the problem. A storm surge model was used to simulate water levels for several synthetic storm events along the coastline of New York City, but did not include any land areas; water levels were extrapolated from the coastline into the city (Aerts et al. 2013). However, a static approach can allow instantaneous (and erroneous) flooding of entire neighborhoods when, for example, water levels at a point on the boundary become higher than a neighborhood flood protection structure (Gallien et al. 2011). Where hydraulic structures are important, they must be explicitly incorporated into the mesh to avoid this problem.

Dynamic approaches have been used in several recent studies of flooding, typically via nesting of higher-resolution simulations. For Hurricane Sandy in New York City, a nested-grid approach was used to simulate high-resolution urban flooding (Blumberg et al. 2015), and an ocean-scale model was coupled to a high-resolution urban inundation model to hindcast the flooding (Wang et al. 2014). A coupled approach was used with the sub-grid

model FloodMap (Yu and Lane 2006), with an emphasis on computational efficiency for an end goal of using the coupled model to simulate many synthetic surge events in a probabilistic way (Yin et al. 2016). A widely used example of the dynamic approach is the LISFLOOD-LP model, which includes only the physical processes that are relevant for predicting inundation extents for riverine floods (Bates and de Roo 2000). Another model, MSN_Flood, has been nested within a storm surge model to provide higher-resolution flooding predictions (Hartnett and Nash 2017; Comer et al. 2017; Olbert et al. 2017).

In comparison with aerial observations, the dynamic approach has been found to outperform the static approach, for both riverine (Bates and de Roo 2000) and coastal flooding applications (Bates et al. 2005; Purvis et al. 2008). It has thus been suggested that static models should be avoided when computational speed is not of primary concern (Ramirez et al. 2016).

However, the difference in computational effort between these approaches has not been quantified, and it is possible that the cost of nested models is prohibitive for forecasting purposes on large domains. For applications with time constraints, there is a need to extend the static approach by using geospatial techniques to represent the dominant physics, such as the use of land cover data to represent friction losses. This hydrologic principle is used in state-of-the-art models such as the Hydrologic Engineering Center's River Analysis System (HEC-RAS) (Liu et al. 2018) and the ADvanced CIRCulation (ADCIRC) model (Bunya et al. 2010), which use resistance factors associated with the Manning equation and based on land cover variations when applied to overland flooding (Kalyanapu et al. 2009). There have been efforts to optimize their use for full-physics, coastal flooding models (Passeri et al. 2011; Mayo et al. 2014; Medeiros and Hagen 2013), but not for a dynamic downscaling.

In this manuscript, we focus on the downscaling of real-time coastal flooding predictions for decision support. It is hypothesized that, by implementing and then extending a downscaling method with geospatial techniques to include the dominant physics, the accuracy of real-time flood predictions will be increased with minimal cost. We consider three methods. In the static method, the water levels at the boundary of the predicted flood extent are extrapolated to intersect with the ground-surface contour in a high-resolution DEM. Then, this method is extended to consider the slope of the predicted flood extent and frictional losses. The methods use an automated, open-source mapping technique that can be applied in real-time on a statewide domain and can post-process model output in less than 15 minutes. Improvements in model accuracy are quantified via comparisons to a full-physics, numerical model simulation with overland resolution identical to that of the DEM. These methods have the potential to improve accuracy for coastal flooding predictions at minimal cost.

2 Hurricane Florence (2018) in North Carolina

2.1 Storm history

Hurricane Florence was chosen as the test-case storm because of its widespread flooding in coastal North Carolina (NC). Florence reached Category-4 strength on the Saffir–Simpson Hurricane Wind Scale as it moved across the Atlantic Ocean, and it made landfall as a Category-1 hurricane in southeastern NC (near Wrightsville Beach) with wind speeds of 40 m/s at 1115 UTC on September 14. During and after landfall, it was a slow-moving

storm with a 9-km/hr westward motion, and its rainfall totals exceeded 1 m in some areas. Florence was downgraded to a tropical storm by 0000 UTC on September 15 while the storm was located just north of Myrtle Beach, South Carolina. From there, the storm moved inland and continued losing energy while traveling north until finally dissipating over Massachusetts shortly after 1200 UTC on September 18 (Stewart and Berg 2019).

In addition to its rainfall-driven flooding, Florence also created storm surge and flooding in coastal NC (Stewart and Berg 2019). The maximum inundation heights were 2.4 to 3 m above ground level along the Neuse River and its tributaries, but the inundation was also 2 m above ground level along the Pamlico River and the open coast of Onslow Bay. Farther south, the inundation was 1 to 1.5 m above ground level in Wrightsville Beach to Cape Fear. These highest inundations persisted for a full tidal cycle, as the storm slowed at landfall.

2.2 Carteret county

Carteret County is part of coastal NC, which protrudes into the Atlantic Ocean significantly compared to surrounding regions of the US coast. The county is located at the southwestern shore of Pamlico Sound, with the Neuse River estuary to the north and the city of Jacksonville and Onslow County to the west (Fig. 1). Carteret County contains the stretch of barrier islands from Ocracoke Inlet in the northeast to Bogue Inlet (at White Oak River) in the southwest. This includes Cape Lookout, which is the middle of the three capes along the coast of NC. It is 1,369 km² in land area and is home to about 66,500 permanent residents as of the 2010 census. The population center of the county is located in the area surrounding Morehead City and Atlantic Beach on Bogue Sound.

Carteret County contains a diverse arrangement of geography and topography. The barrier island system includes islands facing in several directions, and thus includes

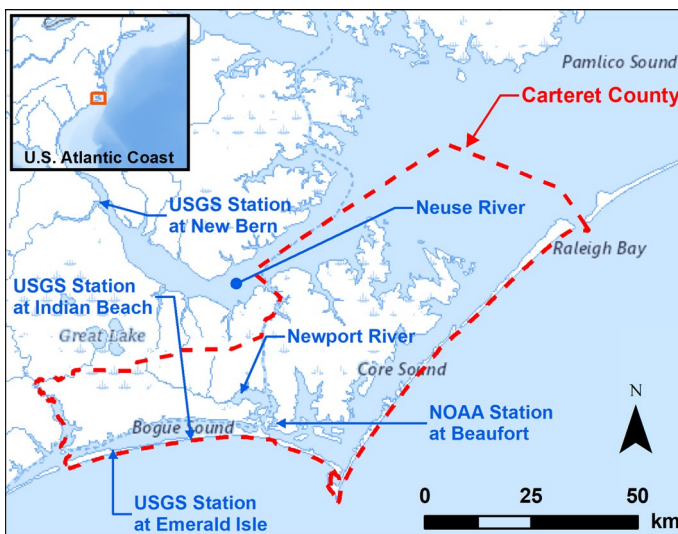


Fig. 1 Location of Carteret County, NC. Notable rivers, bays, and sounds are identified. Also shown are three USGS sensors and one NOAA station, which collected continuous water levels and other data during the storm

back-barrier sounds with varying fetch. Furthermore, while many of the more populated areas along the coast (e.g., Emerald Isle and Morehead City) lie on steeper topography, much of the northeastern region of the county close to Pamlico Sound consists of flat farmland. There are also several river estuaries in Carteret County, including the White Oak River, Newport River, and part of the Neuse River estuary. This physical diversity allows for the downscaling method to be evaluated for a variety of potential coastal environments.

Carteret County was affected greatly by Florence. As the storm approached the coast from the southeast and then made landfall to the southwest, the onshore winds were blowing directly at and across the county. This resulted in elevated water levels along the barrier islands, in the sounds, and in many of the river estuaries in the county and surrounding areas. USGS sensors deployed in downtown New Bern on the Neuse River reached 3 m above NAVD88 (North American Vertical Datum of 1988). A USGS sensor installed in a wave-protected area of Emerald Isle on Bogue Sound (also in Carteret County) measured a peak water level of 2.4 m above NAVD88 (Stewart and Berg 2019). The impact of Florence on Carteret County and NC reinforces the need for fast and accurate predictions of coastal flooding to aid decision-makers as storms approach the coast.

3 Methods

3.1 Geospatial data and software

3.1.1 DEMs and land cover data

Each downscaling method requires raster data that are appropriate for the given study area. Digital Elevation Models (DEMs) are derived from surveys and are available at high resolutions. This research uses a DEM obtained from NC Emergency Management (NCEM) that covers 32 NC coastal counties (Fig. 2). It was derived from the Quality Level 2 LiDAR survey of NC in 2014 and has a 15 m (50 ft) resolution with a total of 430 million raster cells (Tull 2018). To facilitate analyses in Carteret County, a smaller DEM was extracted with only the extents of the county (Fig. 2), as well as adjacent water sources. This smaller DEM was then used to increase resolution in Carteret County in the storm surge models, while only the portion within Carteret County (Fig. 2, bottom, outlined in red) was used to calculate flooded areas to analyze the performance of the downscaling methods.

The head loss frictional method also requires a raster of land cover classifications that can be converted into friction coefficients. The source used in this research is the National Land Cover Database (NLCD), which provides nationwide (US) data on land cover at 30-m resolution and classifies land cover into 16 types (Fig. 3). These data can be downloaded for multiple years, with 2016 being the most recent year (Multi-Resolution Land Characteristics Consortium 2019). Because these data are given at a lower resolution than the DEM, nearest neighbor interpolation is done to increase the raster resolution to match the DEM.

3.1.2 GRASS GIS

GRASS (Geographic Resources Analysis Support System) GIS is an open-source software (GRASS Development Team 2017). We use GRASS GIS to implement the downscaling, because it can be automated using Python scripts and is efficient at processing raster data.

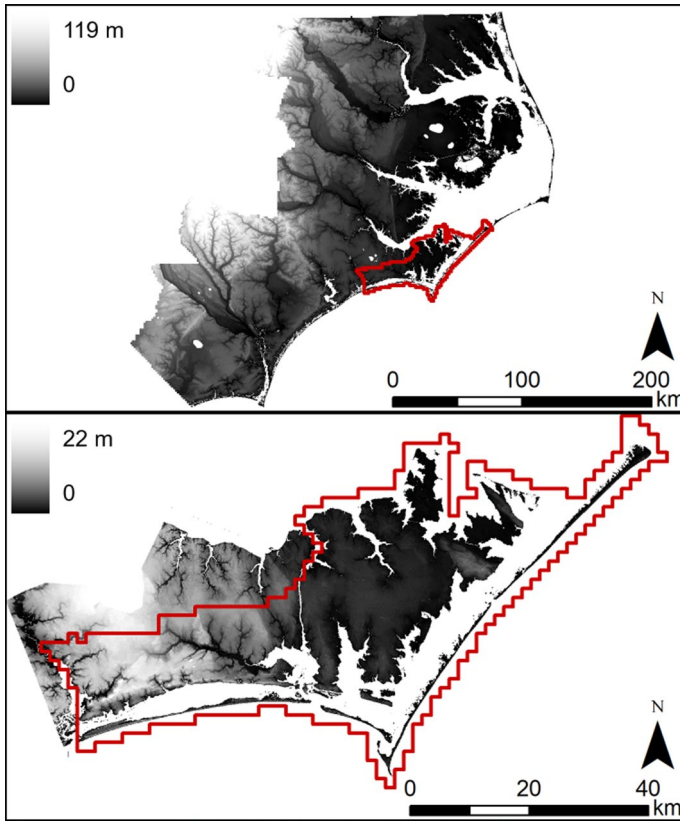


Fig. 2 DEMs used in downscaling. The top figure is the DEM obtained from NCEM that represents 32 NC coastal counties at 15-m resolution, where the red outline represents the DEM shown in the bottom figure. The bottom figure is the portion of the DEM used in downscaling water levels for Carteret County. The red outline in the bottom figure shows the extents of the DEM used to create the NC9-Carteret mesh and to calculate for flooded areas

GRASS GIS data are organized into “locations,” which are directories containing all project data, and “mapsets,” which are subdirectories in the location. All data within one location are registered to the same coordinate reference system (projection, datum, units, etc.). We use NC state plane coordinate system EPSG 2264 (units of US survey feet, horizontal datum of the North American Datum 1983) to perform the distance measurements more efficiently than when using the geographic coordinate reference system with latitude and longitude in degrees. These methods utilize built-in GRASS GIS functions to extrapolate raster data, perform numerical calculations, and convert results to a more user-friendly format.

3.2 Models for coastal flooding in NC

Florence’s potential effects on coastal flooding were predicted by researchers using the ADvanced CIRCulation (ADCIRC) model (Westerink et al. 1992, 2008). This study

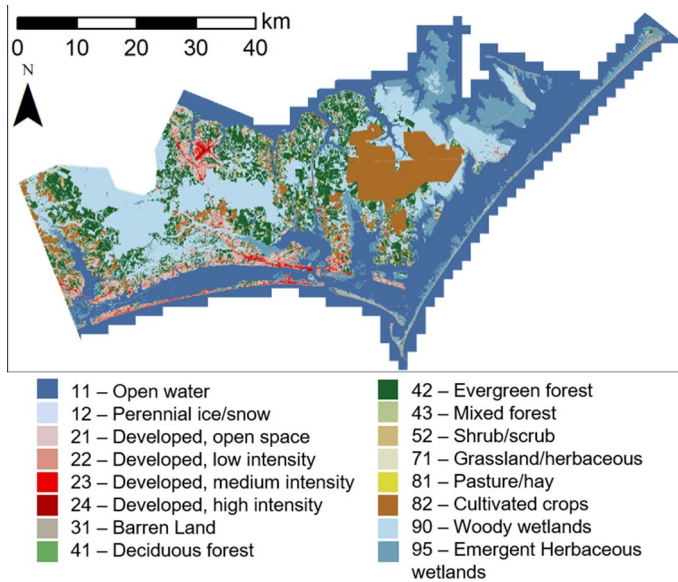


Fig. 3 Land cover raster. The land cover raster used in this study is shown, which is a portion of the NLCD 2016 raster, extracted to the extents of the DEM used in downscaling. Each land cover classification has an assigned integer value and color

examines ADCIRC simulations used on two unstructured meshes: one used currently for forecasting in NC and one with higher resolution used for validation of the downscaling methods discussed in this manuscript.

3.2.1 ADCIRC

ADCIRC is tightly coupled with the Simulating Waves Nearshore (SWAN) model for wave and storm surge applications (Booij et al. 1999; Zijlema 2010; Dietrich et al. 2011b) and has been validated extensively in studies along the U.S. Gulf and Atlantic coasts (Dietrich et al. 2012a; Hope et al. 2013; Sebastian et al. 2014). In hindcasting studies that use highly accurate, data-assimilated wind fields, ADCIRC can achieve accuracy for water levels with a mean absolute error less than 25 cm (Dietrich et al. 2011a). In this study, the tightly coupled ADCIRC+SWAN was used for forecasts and hindcasts, with SWAN settings similar to recent studies (Dietrich et al. 2018). However, because our focus is the downscaling of coastal water levels, we refer to ADCIRC for simplicity.

ADCIRC was used for forecasts of 5 days with a time step of 0.5 seconds, and then hindcasts of 11.5 days with a time step of 0.25 seconds. Advective transport terms were disabled; bottom drag was represented with a depth-dependent quadratic friction law with spatially varying Manning's n values and a lower limit on the bottom drag coefficient of $C_f = 0.003$ for the forecasts and $C_f = 0$ for the hindcasts; and air-sea momentum transfer was represented via the relationship from Garratt (1977) with an upper limit on the surface drag coefficient of $C_D = 0.0028$ for the forecasts and $C_D = 0.002$ for the hindcasts, similar to previous studies (Dietrich et al. 2011a, 2012b). Spatially varying horizontal eddy viscosity for the momentum equations was set to $10 \text{ m}^2/\text{s}$ in open water and $2 \text{ m}^2/\text{s}$ over land. The eddy viscosity for hindcasts was set to $20 \text{ m}^2/\text{s}$ over land within Carteret County

where resolution has been increased in the NC9-Carteret mesh. Wind fields for predictive ADCIRC simulations are generated from a parametric vortex model (Gao 2018), which uses parameters given by National Hurricane Center (NHC) forecasts to develop fields for surface pressures and wind speeds that are temporally and spatially varying (Dietrich et al. 2018).

In forecasting applications, ADCIRC is automated via the ADCIRC Prediction System (APS), which is a scripting system designed to run ADCIRC simulations and deliver real-time predictions of storm surge (Fleming et al. 2008; Dresback et al. 2013; Dietrich et al. 2013). The APS now operates for all tropical cyclones that threaten the US coast. During Florence, the APS was run in real-time using the forecast advisories from the NHC; these advisories are issued at least every 6 hr and consist of a 5-day forecast of parameters for the storm size, intensity, and location. The APS is designed to automatically download storm parameters from the NHC guidance and apply them to the operational ADCIRC model. Results from these simulations are shared directly with decision-makers, as well as shared publicly via web sites such as www.cera.coastalrisk.live.

3.2.2 Unstructured meshes

This study will consider ADCIRC results on two unstructured meshes: the existing mesh for forecasting in NC (referred as NC9), and a new mesh with higher resolution in Carteret County (referred as NC9-Carteret).

ADCIRC represents the complex coastal environment with an unstructured mesh of finite elements, which can vary in size to represent geographic features at a variety of spatial scales. The mesh used for real-time storm surge prediction in NC during Florence was the NC v9.98 (NC9) mesh (Blanton and Luetlich 2008). Coastal flooding predictions with this mesh have been well-validated (Blanton and Luetlich 2010; Cyriac et al. 2018). The mesh consists of 622,946 vertices and 1,230,430 triangular elements that cover the entire Western North Atlantic Ocean, Gulf of Mexico, and Caribbean Sea, although most of the elements are concentrated in NC (Fig. 4, left column). The mesh resolves inland areas only for NC, while other coastlines in the domain are modeled as no-flow boundaries with a tangential-slip boundary condition. Bathymetry and topography in the NC9 mesh were developed from several DEMs describing the NC coastal regions (Blanton et al. 2008), and the ground elevations are relative to NAVD88. More than 90 percent of elements in the NC9 mesh are located in coastal NC. NC9 mesh resolution is sufficient for conveying flow along the coast, into estuaries and onto floodplains (Westerink et al. 2008; Dresback et al. 2013). Element sizes range from about 10 to 100 km on a side in the deep Atlantic Ocean to as small as about 15 to 25 m near Oregon Inlet and Cape Fear River, but elsewhere the smallest elements are generally on the order of 100 to 200 m along barrier islands and other inlets. Resolution is relaxed in the Pamlico and Albemarle Sounds, with element sizes larger than 1500 m in open water.

Because the NC9 mesh must be able to represent flooding anywhere in NC and with reasonable simulation times, it does not represent hydrodynamics on smaller, infrastructure-level scales (about 15 m). To evaluate the performance of the downscaling methods, we compare a version of the NC9 mesh with higher resolution in Carteret County (Fig. 4, right column). To enable a direct comparison, the NC9 mesh is refined so its overland resolution is equal to the resolution of the DEM (15 m). As a result of this one-to-one conversion, NC9-Carteret appears as a structured grid with each square cell bisected diagonally to create a large set of identical, isosceles triangular elements, each with two 15-m edges.

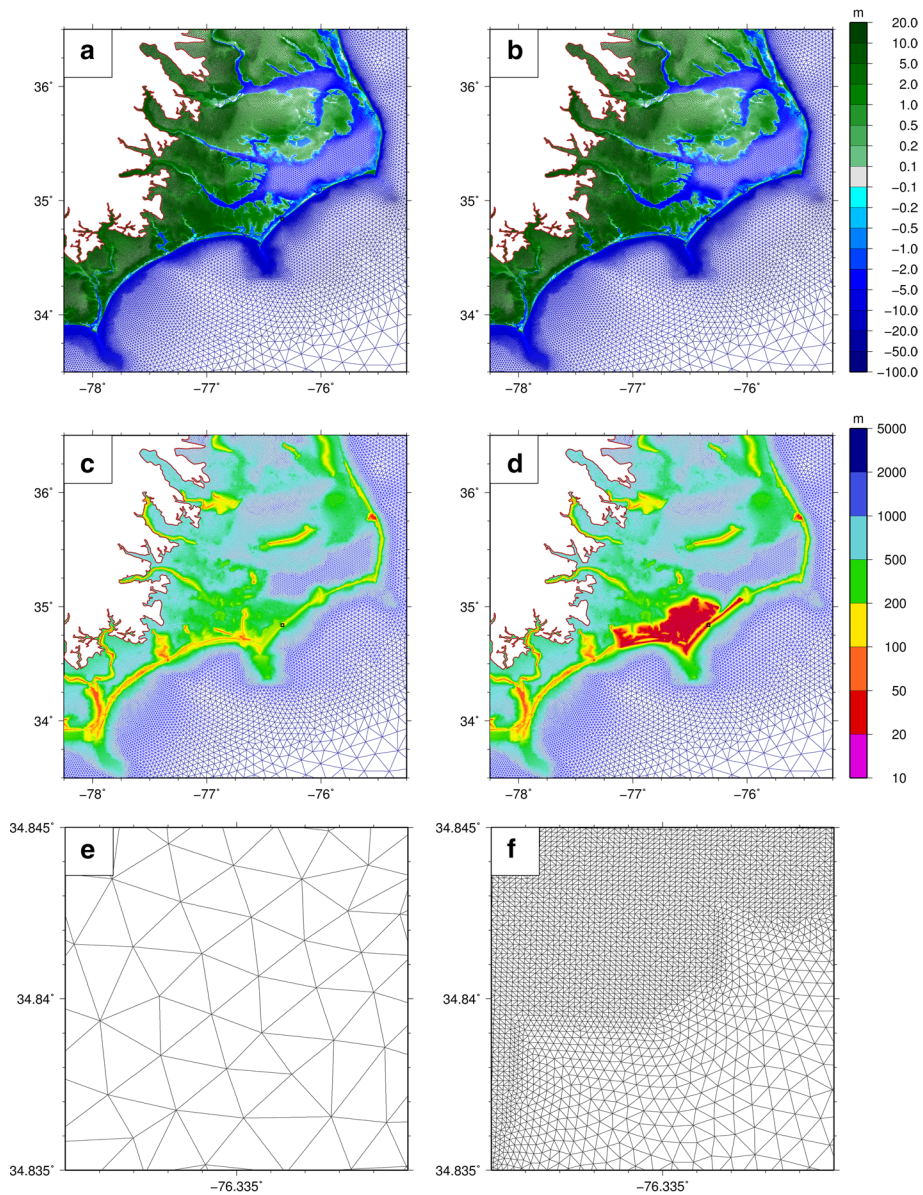


Fig. 4 Finite element meshes for coastal North Carolina: (left) NC9, and (right) NC9-Carteret. Panels are **a**, **b** bathymetry and topography (m relative to NAVD88), **c**, **d** vertex spacing (m), and **e**, **f** meshes in a zoom along the Cape Lookout National Seashore. Note the higher resolution in Carteret County in panel **d**, and the transition to 15-m elements in panel **f**.

This is the case only for the dry-land elements in Carteret. In the surrounding areas, the mesh becomes flexible as it transitions to larger elements to match the NC9 mesh. The final mesh contains 6,772,170 vertices and 13,528,879 elements—almost 11 times larger than NC9. We refer to this refined mesh as NC9-Carteret. Such a mesh is too expensive to use

operationally, but we can use it for a high-resolution ADCIRC hindcast of Florence. We assume these high-resolution model results are “truth,” in that they include a full-physics representation of coastal flooding due to the storm.

3.3 Downscaling methods

We consider three methods (Fig. 5) for downscaling the flood extents: (1) “static,” in which the water is extrapolated as a flat surface until it intersects with the ground surface; (2) “slopes,” in which the extrapolation uses the local water surface slope; and (3) “head loss,” in which a land cover dataset is used to represent frictional dissipation of overland flooding.

3.3.1 Static

In the static method, the ADCIRC-predicted flood extents are enhanced by: (1) interpolating (downscaling) the maximum water levels from the mesh points to a raster at the same resolution as the high-resolution DEM, (2) extrapolating this water-level raster as a flat surface until it intersects the ground surface of the DEM, and (3) enforcing a hydraulic connectivity condition.

The predicted flood extents are represented in the ADCIRC output as the maximum water levels during the simulation. For vertices that were flooded, the water level is provided; for vertices that remained dry, a “null” value is provided. The water levels are first downscaled to a raster with the same resolution as the DEM: 15 m for the NC DEM used in this study. Then, the raster of maximum water levels is extrapolated to intersect with the ground surface in the DEM. This extrapolation is achieved by using the GRASS GIS module *r.grow* (Larson and Clements 2008), which expands an input raster into neighboring null regions by a specified number of cells (referred to as the radius). The new, “grown” cells are given the value of the closest cell in the original

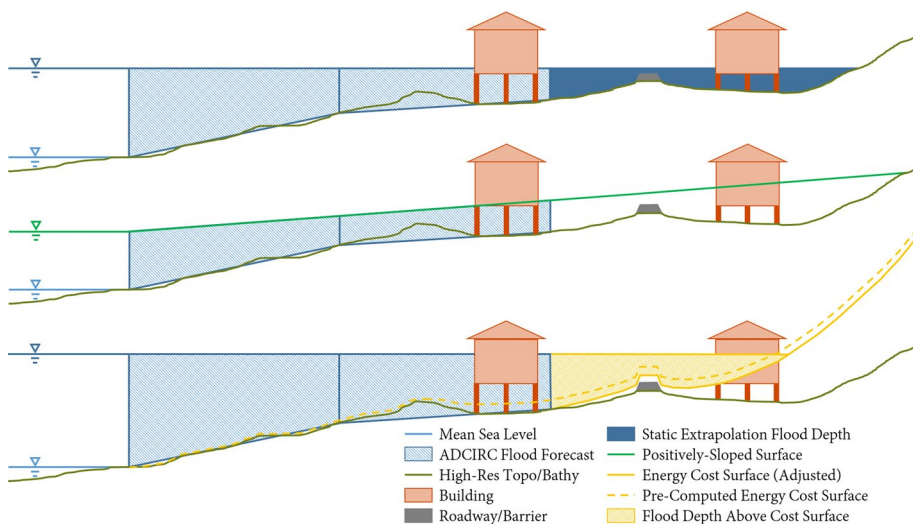


Fig. 5 Schematic showing a side view of each downscaling method: (from top to bottom) static, slopes, and head loss

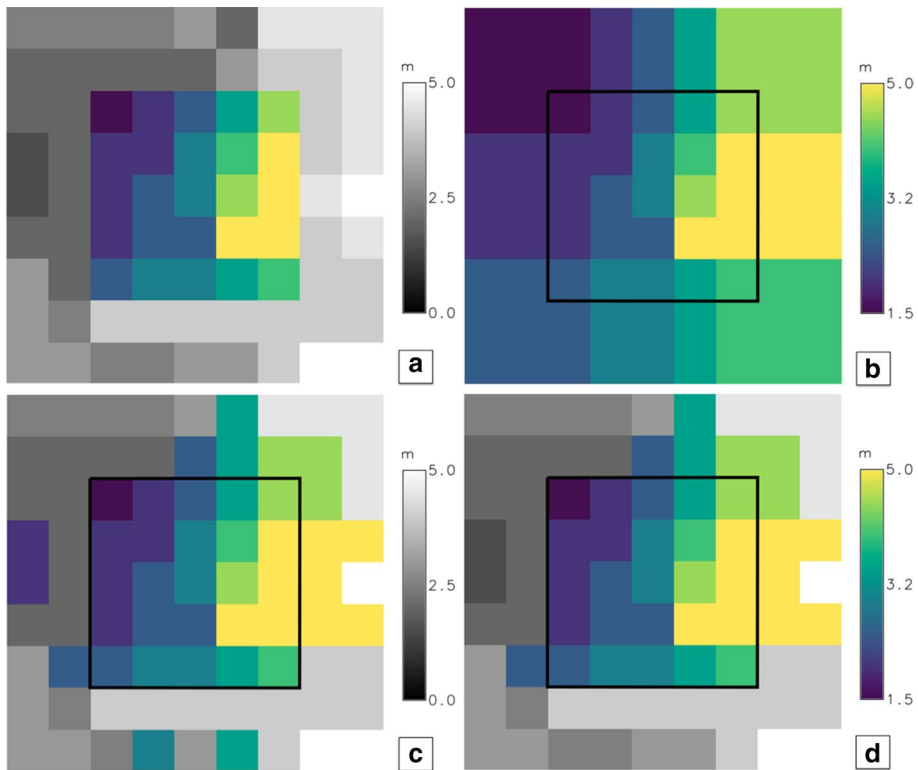


Fig. 6 Conceptual illustration of the `r.grow` module using a radius of two raster cells, and how it was modified to incorporate an elevation check. **a** Raster of water levels (color) at the same resolution as the underlying DEM (gray scale). The black line in the following figures indicates the boundary of this original raster. **b** Raster expanded using the original `r.grow` module in GRASS GIS. **c** Result of using the modified `r.grow` to incorporate an elevation check with the DEM. **d** Final result, where new, “grown” cells are retained only if their value is greater than that of the corresponding DEM cell and if it is connected to the original raster

raster (Fig. 6a, b). For this study, the `r.grow` module was modified to accept both an input map (maximum water levels) along with a base map (DEM), and an additional criterion was added so the grown cells are retained in the output raster only if the input value is greater than the base value at the same location (Fig. 6c). This is a one-to-one comparison, as the resolution of the two rasters is identical, and it ensures that flooding is extended only to the ground surface. It is noted that the “radius” can be specified by the user, and it will vary by application due to variations in mesh resolution and local topography. In our analyses below, we use a radius of 30 cells (about 450 m), which is representative of typical NC9 element sizes along its wet/dry front.

Then, a hydraulic connectivity condition is enforced. After extrapolation, the new raster may contain wet cells that are unconnected to the original raster (Fig. 6c). This can happen when flood waters are grown past a higher feature (such as a dune) and into a lower area (such as a neighborhood), and it is an undesirable result. To fix this, other GRASS GIS modules (`r.clump`, `r.reclass`, `r.mapcalc`) are used to identify groups of new,

isolated raster cells and then remove them Shapiro and Metz (2008), Westerveldt and Shapiro (2008), Shapiro and Clements (1991).

The resulting flooded surface has effectively been extended farther overland to where the water elevations intersect with the land elevation. In some locations, this extrapolated distance may be as large as 450 m (such as in a small-scale coastal river), while in others, it is not changed at all (Fig. 6d).

Consider an example for a portion of a barrier island in Carteret County (Fig. 7). The difference in resolution is significant between the DEM (Fig. 7a) and the ADCIRC-predicted water levels (Fig. 7b). Strong winds are blowing from the northwest (upper left), causing a surge of more than 2 m on the sound side of the island, while the maximum water levels are about 1 m on the ocean side (lower right). In the southwest (lower left), there is predicted overtopping where the island topography is relatively low, while in the northeast (upper right), the higher dune is preventing the surge from moving over the island. The coarser mesh resolution does not allow the sound-side surge to push over the island and against its dune, and it prevents water on the ocean side from approaching the mean shoreline. When the water levels are downscaled and extrapolated (Fig. 7c), more of the island is flooded on both the sound and ocean sides, and only the dune crest is dry.

3.3.2 Slopes

The slopes method is similar to the static method, but it accounts for the slope of the predicted water surface. By creating a continuous raster surface from the water levels at each ADCIRC vertex, slopes can be calculated throughout the raster. These slopes can then be used in downscaling to add or subtract from the elevation of the horizontally extrapolated water surface.

To compute slopes from the predicted water surface, it is essential to have a continuous raster. A regularized spline with tension (Mitas et al.; Mitasova et al. 2005), implemented in GRASS GIS as module `v.surf.rst`, is used to interpolate the ADCIRC output onto the high-resolution raster. The water surface is interpolated, but rasters are also created with the slopes of the surface in both the x (east–west) and y (north–south) directions.

Then, these rasters are used to extrapolate the water surface. First, the rasters are grown, regardless of the ground surface, so that all null cells have values for the nearest water

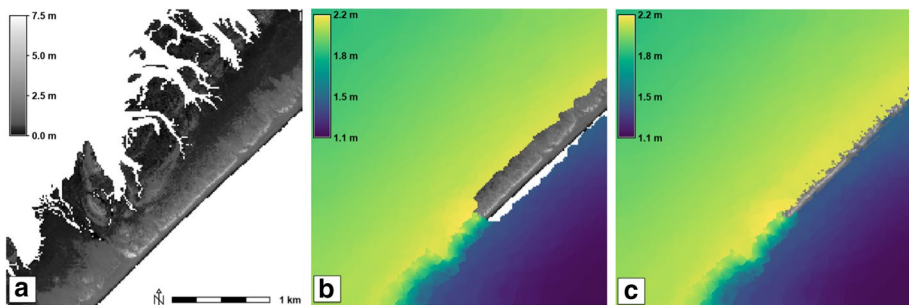


Fig. 7 Test case on small section of barrier island in Carteret County, NC. **a** DEM for Carteret County barrier island, 200×200 cells or 3×3 km. The dune crest is evident by the lighter shades. **b** ADCIRC water level raster superimposed on DEM. Visible white area represents water not reaching the mean shoreline on the ocean side. **c** ADCIRC raster after running the modified `r.grow` process, where flooding is extended farther over land to where it intersects the DEM

surface and slopes. Then, new water elevations are determined by a simple function of the slope multiplied by the horizontal distance traveled, added to the static value:

$$\zeta_{\text{slopes}} = \zeta_{\text{static}} + c m_x \Delta x + c m_y \Delta y \quad (1)$$

where ζ_{slopes} is the water level at a null cell as computed with the slopes method, ζ_{static} is the water level at the same null cell as computed with the static method, c is a slope exaggeration multiplier (set to 1 for this study), m_x and m_y are the slopes in the x and y directions, and Δx and Δy are the distances in the east–west and north–south directions.

The slopes method is similar to the static method in that both are a series of `r.grow` operations and raster calculations. Because the slopes method must consider horizontal distances and slopes in both the x and y directions after computing a continuous raster surface using splines, this method is more computationally intensive than the static method.

3.3.3 Head loss

In the head loss method, the downscaled flood extents are modified due to frictional dissipation as derived from land cover data. Instead of extrapolating the water surface to a DEM surface, the head loss method extrapolates to an energy cost surface, which represents the total energy required (elevation plus head loss) to reach a flood extent.

In ADCIRC, along with many other hydraulic models, the amount of friction associated with land cover is represented using Manning’s n coefficient. These values are assigned by using data from the USGS National Land Cover Database (NLCD). Relating these land cover classification values to a specific Manning’s n coefficient is a common research topic, and there is a range of acceptable n values for each classification (Liu et al. 2018; Kalyanapu et al. 2009). These values are then developed into a bottom drag coefficient for use in the momentum conservation equations.

In this study, we use a modified form of Manning’s equation, which can be manipulated to directly calculate head loss in overland flow (Rubin and Atkinson 2001):

$$h_L = L \left(\frac{nU}{kR^{2/3}} \right)^2 \quad (2)$$

where h_L is head loss, L is a lateral distance, n is Manning’s coefficient, U is the flow velocity, k is a unit conversion ($k = 1$ for SI units; $k = 1.49$ for US customary units), and R is the hydraulic radius. In overland flow, the hydraulic radius R can be approximated as the depth of flow. Using values for the other flow variables, the head loss can be determined over each raster cell.

However, there are two issues that arise when applying this method to forecasting: (1) water velocities and flow depths are unknown prior to receiving input from ADCIRC; and (2) cumulative head loss must be calculated based on an accumulation of frictional losses over the flow paths, which are unknown. To overcome these issues, the GRASS GIS module `r.walk` (GRASS Development Team 2002) is used to pre-compute an energy cost surface that contains both gains in potential energy due to elevation changes in the DEM and head losses due to surface friction associated with land cover classifications.

The `r.walk` module creates a raster map showing the anisotropic cumulative cost of moving between different geographic locations. In this study, cost represents the total energy needed to reach a given location based on both elevation changes and head loss due to land cover. The `r.walk` module creates a series of “least cost paths,” over which

accumulation of head loss is calculated until a full raster is created containing the “least cost,” in terms of energy head, from MSL to any point throughout the raster. By carefully choosing `r.walk` parameters, each raster cell will be calculated as:

$$\text{cost}_{\text{total}} = \Delta z + \sum L \left(\frac{nU}{kR^{2/3}} \right)^2 \quad (3)$$

where Δz is based on the given DEM, L is built-in to the `r.walk` calculations, and the full second term on the right-hand side of the equation is the cumulative head loss from Eq. 2. During the pre-computational phase, U and R are unknown without input water velocities and elevations from ADCIRC. Therefore, a constant ratio of $U/R^{2/3}$ is assumed in the pre-computational process to entrain flow paths based on both elevation and friction losses. This leads to a raster only containing the “raw cost” in the form of:

$$\text{cost}_{\text{raw}} = \sum L \left(\frac{n}{k} \right)^2 \quad (4)$$

This raw cost raster is the cumulative head loss based on flow paths, and it is pre-computed. Then, during the downscaling process, the total cost raster (Eq. 3) is developed by using the raw cost raster, U and R values imported from the ADCIRC predictions, and the ground surface from the DEM. The predicted water surface is then extrapolated to the energy surface, as represented by the total cost raster.

We note two aspects related to the values of U and R obtained from ADCIRC. First, ADCIRC treats the wet/dry front as a no-normal-flow boundary, and thus its computed water velocities are negligible at the front. Thus this study assumes a constant value of $U = 1 \text{ m/s}$. Second, the hydraulic radius R is approximated by the water depth, but ADCIRC has already considered losses due to frictional dissipation in its overland flow calculations. Thus it is necessary to adjust the total cost raster to account for these energy losses. This allows the water levels to be compared in terms of depths above the energy cost surface, rather than depths above the topographical surface.

In summary, a version of Manning’s equation (Eq. 2) has been introduced into the downscaling method to account for energy head loss due to land cover friction. Rather than extrapolating water elevations to a DEM surface, they are extrapolated to an energy surface. Flow paths accounting for accumulation of head loss are pre-computed using the GRASS GIS module `r.walk` (Fig. 8a). When maximum water elevation forecasts are received from ADCIRC (Fig. 8b), they are used to identify the losses due to frictional dissipation that were considered already in its overland flow calculations (Fig. 8c). When the ADCIRC-predicted water surface is extrapolated horizontally to populate the null raster cells (Fig. 8d), the cost overcome by ADCIRC within the given extent is also extrapolated (Fig. 8f). This allows the water levels to be compared in terms of depths above the energy cost surface, rather than depths above the topographical surface. The resulting water surface is downscaled to consider energy head losses due to friction in overland flooding (Fig. 8g).

3.3.4 Implementation for real-time forecasting

Beginning with the 2017 hurricane season, the static method was used in real-time to enhance the resolution of flooding predictions for NC. Due to prohibitive run times, it was necessary to parallelize the method and run it on a high-performance computing (HPC)

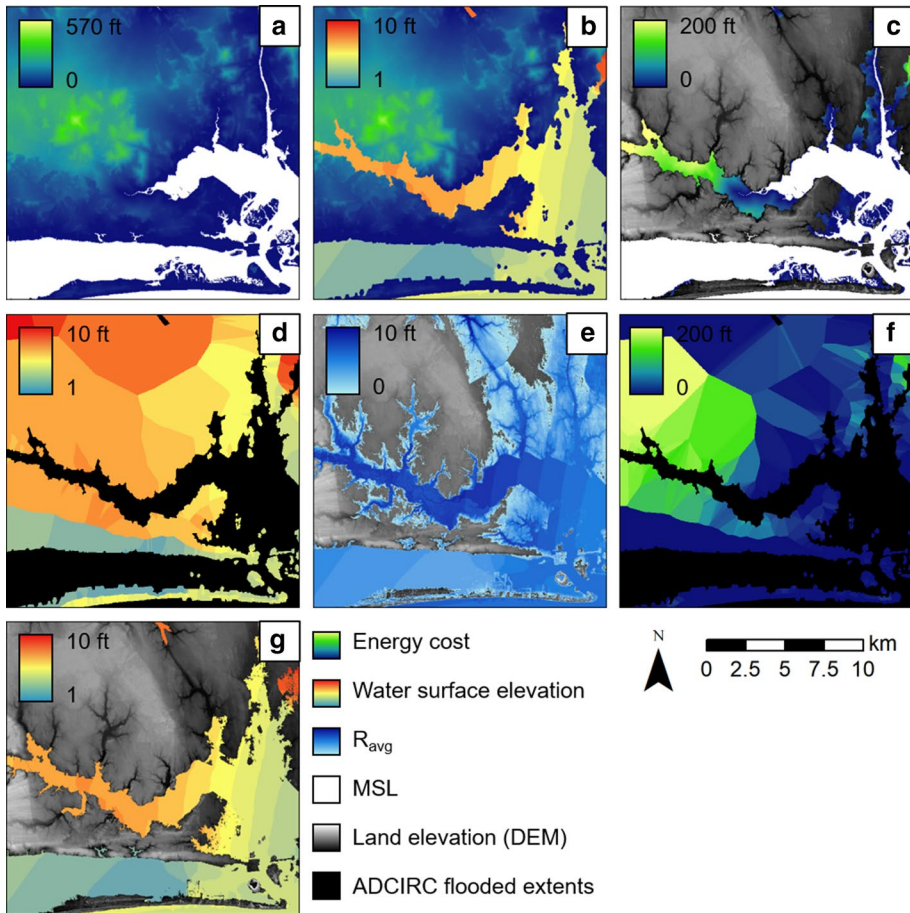


Fig. 8 Sequence of raster operations for the head loss method: **a** pre-computed raw cost raster, with MSL denoted by the white regions; **b** ADCIRC maximum water levels; **c** energy costs included in the ADCIRC flood calculations; **d** horizontal extrapolation of ADCIRC water levels; **e** hydraulic depths R_{avg} ; **f** horizontal extrapolation of energy costs included in the ADCIRC flood calculations; and **g** the final downscaled water surface

cluster, using 16 cores (Tull 2018). The parallelized method was tested using the daily ADCIRC predictions from the APS, and was subsequently used to post-process APS simulations for each advisory of Hurricanes Harvey, Irma, Jose, and Maria, and Tropical Storm Philippe. Although these storms caused minimal to no effects in NC, they were important for testing the functionality and robustness of the method. In 2018, the method was used to downscale the flooding predictions for Hurricanes Florence and Michael, both of which caused flooding in NC. For all storms during these seasons, the ADCIRC-predicted flood extents from the $\sim 600,000$ -vertex NC mesh were downscaled to the $\sim 400,000,000$ -cell DEM. The method required between 11 to 14 minutes for simulations with minimal predicted flooding, and 15 to 20 minutes for simulations with extensive predicted flooding.

For the 2019 and ensuing hurricane seasons, the static method was adjusted to eliminate all NC-specific hard-coding and the need for parallelization. It now requires between 25 to 35 minutes to process real-time simulations for Hurricane Dorian. Although the

updated method was slower, this timeframe met the needs of emergency managers in NC and elsewhere. Downscaled results have been distributed to NC Emergency Management in shapefile format, using water surface elevation binning intervals of 0.15 m. In 2018 and 2019, statewide inundation-depth rasters were also produced for both state and federal emergency management. ADCIRC forecast guidance will continue to be downscaled and shared with stakeholders in upcoming hurricane seasons, including the new capability to downscale using the head loss method.

4 Model validation

The ADCIRC predictions were validated for a hindcast of Florence. The atmospheric forcing was based on the generalized asymmetric Holland model (Gao 2018; Dietrich et al. 2018), but used best-track information released after the storm (Stewart and Berg 2019). Predicted water levels on the NC9 mesh are validated using high-water marks (HWMs) throughout coastal NC and hydrographs at four stations near Carteret County (Fig. 9). A total of 431 HWMs were collected after the storm (U.S. Geological Survey 2020); of these, only 84 HWMs were due to storm surge. A total of 58 points were considered in this study because 26 of the previous 84 points lie outside the extents of the NC9 simulation and cannot be used as a direct comparison. The ADCIRC predictions are a good match to the HWMs, with a correlation coefficient of $R^2 = 0.897$ and 38 points (65.5 percent) within 10 percent of the observed peak.

Time series of water levels are also represented at four stations, each representing a different geographical dynamic. At the open-water station at Beaufort, the predicted water levels are a close match to the timing and magnitude of the elevated water levels. At the sound-side stations, the peak magnitude is matched closely at Indian Beach but the predictions are low by about 0.5 m at Emerald Isle. At the riverine station at New Bern, the predictions are too high by about 0.5 m, likely caused by inaccuracies in the atmospheric forcing from the parametric vortex model, which may not represent the storm structure in far upland regions. Together, these HWM and hydrograph comparisons show a good match to the peak water levels during the storm, which will be the focus on the downscaled flooding extents.

5 Results

We evaluate the performance of the downscaling methods by considering their representation of coastal flooding due to Florence. First, we evaluate the static method, which has been operational since the hurricane season of 2017, by examining its effects on the flooding predictions for coastal NC over several forecast advisories as the storm approached its landfall. Then, we evaluate all three methods, by comparing their predictions in a hindcast of flooding in Carteret County.

5.1 Performance of static method during Hurricane Florence

Florence made landfall in NC at 1115 UTC on 14 September. By that time, the NHC had issued 60 forecast advisories. Using those storm forecasts, the APS issued guidance starting with Advisory 46, when the storm was first predicted to affect NC. For each APS

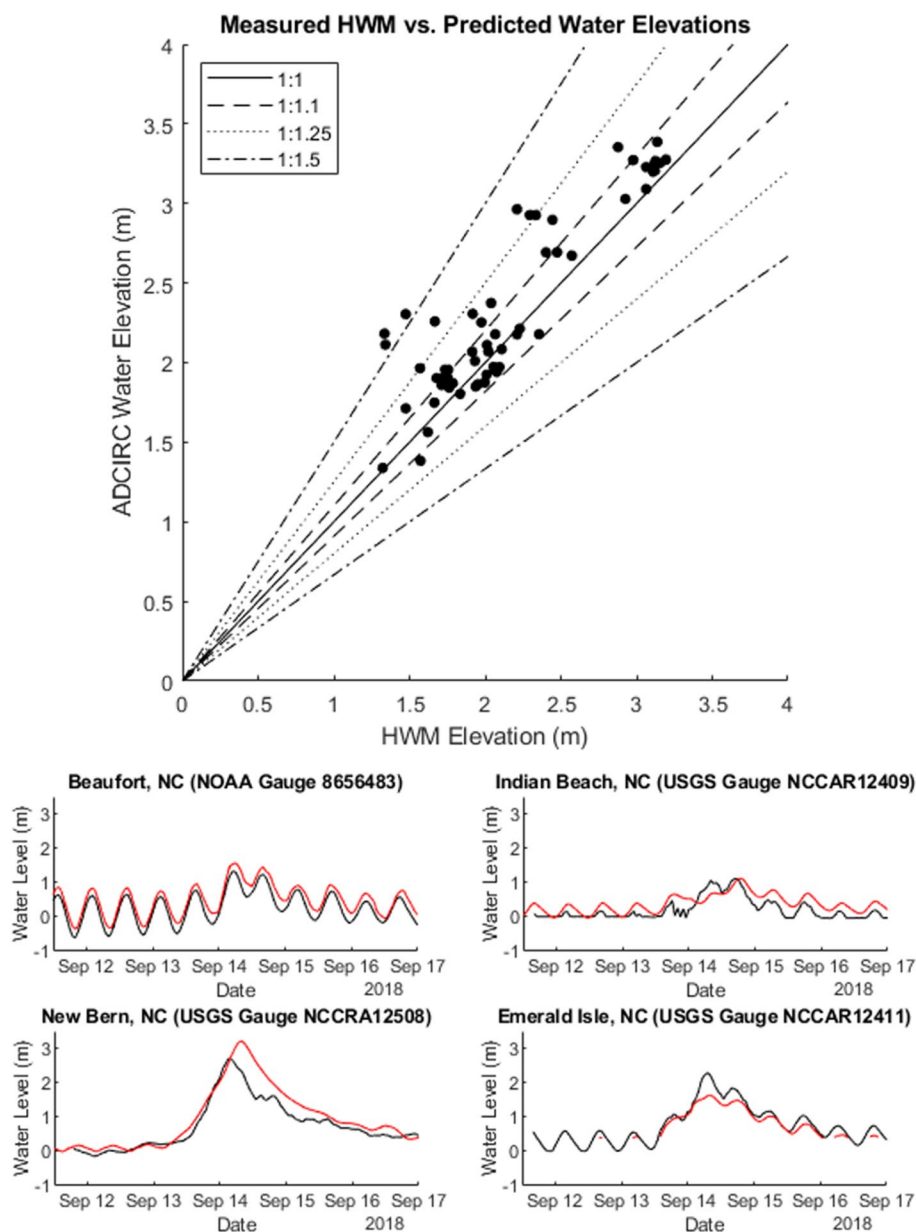


Fig. 9 Comparison of observed and predicted water levels. (Top) Observed high water marks are compared to peak values from the ADCIRC hindcast on the NC9 mesh. Each point represents a point comparison, with lines representing various ratios of observed and predicted water levels. (Bottom) Four hydrographs at stations near Carteret County. Observed water levels are shown in black, and water levels predicted by ADCIRC at the location are shown in red

flood forecast, a downscaled guidance product was generated automatically with the static method. For this analysis, we consider four forecasts:

- Advisory 46, issued 2100 UTC on 10 September, about 86 hr before landfall
- Advisory 50, issued 2100 UTC on 11 September, about 62 hr before landfall
- Advisory 54, issued 2100 UTC on 12 September, about 38 hr before landfall
- Advisory 58, issued 2100 UTC on 13 September, about 14 hr before landfall

Because Advisory 46 was issued 86 hr before landfall, when the storm was roughly 930 km northeast of Puerto Rico and approximately equal in latitude to Miami, Florida, there was more uncertainty in the storm track compared to later advisories. It had a predicted landfall north of Wilmington but southwest of Carteret County (Fig. 10a-1). As the storm approached (Fig. 10b-1, c-1, and d-1), the predicted track shifted to the southwest, closer to its true landfall. Accordingly, peak coastal surges shifted southwest from Carteret County toward Wilmington. The APS predicted the maximum water levels to increase at the inland (west) end of the Pamlico Sound and up the Neuse River estuary to the city of New Bern (Fig. 10b-1 to d-1). New Bern experienced some of the most extreme storm surge during Florence. There was a decrease in the maximum wind speeds over these advisories, but the radius to maximum winds was predicted to increase, and thus the storm affected a larger region as it approached. For example, the predicted storm surge increased at the Cape Lookout National Seashore (black boxes and zooms in Fig. 10).

From Advisory 46 to 50, the water levels increased on both the sound side near Harker's Island (Back Sound) and the ocean side at Cape Lookout National Seashore. The static method extended the predicted flooding (shown in colored contours in Fig. 10) beyond the extents from the ADCIRC simulations (shown in a black outline). The downscaled flooding was extended slightly farther inland on Harker's Island and significantly farther inland on the uninhabited Brown's Island just to the north. This difference was due to the lower average elevation of Brown's Island. The same effect was visible at the barrier island, where water levels were higher on the ocean side than the sound side.

The water levels were predicted to increase in Advisory 54 (Fig. 10c) with complete inundation of Brown's Island. Thus, the downscaling had no effect, as there was no dry land across which to extrapolate water levels. Even with higher water levels, there was still little difference in flooding extent at Harker's Island for Advisory 54. On the ocean and sound sides of the barrier island, the higher water levels did not lead to much difference in horizontal flooding extent. By Advisory 58 (Fig. 10d), the storm was less than a day from making landfall, and predicted water levels on both sides of Cape Lookout were at their highest. Brown's Island was still predicted to be fully inundated, and only minor changes in the flooding extent at Harker's Island were detectable. The barrier island, however, was completely inundated (Fig. 10d-2) due to water elevations of more than 3 m on the ocean side. As with Brown's Island, there were no further effects of the downscaling at this location.

Differences in total flooded area between the ADCIRC model and the static downscaling method for each of these four advisories in Carteret County are shown in Table 1. Although there is no comparison to observations or hindcasts here, the differences in flooded area show how the predictions and effect of downscaling changed as the storm approached NC. There was a general increase in flooding from Advisory 46 to 58, as the downscaled flooded areas increased from 735 to 809 km². But the effect of the downscaling was reduced, as the additional flooded area decreased from 12.3 to 6.9%. These flooded areas show the high-level changes in the predictions due to

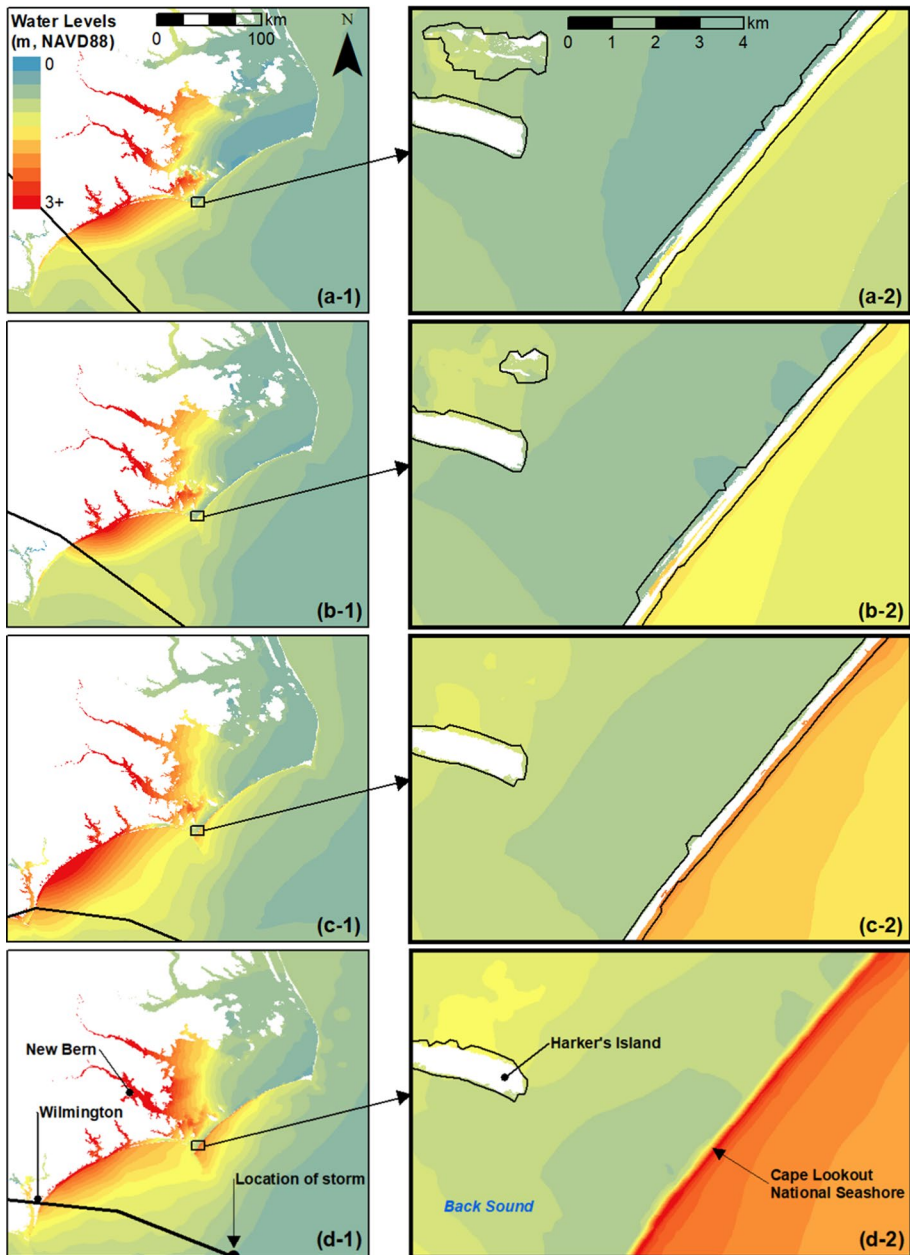


Fig. 10 Daily evolution of Hurricane Florence storm surge predictions from **a-1** 10 September (Advisory 46) to **d-1** 13 September (Advisory 58), where the black lines indicate the predicted track for that advisory. Panels **a-2** through **d-2** show the differences between the enhanced resolution flooding (colored polygons) and the original ADCIRC flooding boundary (black outline)

Table 1 Comparison of predicted flooded area in Carteret County, NC, for Hurricane Florence Advisories 46, 50, 54, and 58, as well as differences due to the static downscaling

Advisory	ADCIRC (km ²)	ADCIRC Static Downscaled (km ²)	Change (%)
46	655	735	12.3
50	688	763	10.9
54	693	757	9.3
58	756	809	6.9

changing forecast information (e.g., storm location, wind speeds, etc.), as well as the effect of the downscaling on the predictions.

5.2 Comparison of downscaling methods in hindcast

The three downscaling methods are evaluated for their accuracy in representing the true flooding extents during Florence. Using the best-track information, we run simulations with ADCIRC on both the NC9 and NC9-Carteret meshes. We assume the NC9-Carteret results are the “truth,” in that they include the full physics of overland flooding at the same resolution (15 m) as the DEM. The NC9 results are then downscaled and compared to the true flooding extents.

Although these simulations are run for a hindcasting format in which computational time is less important, each downscaling method was created to use in forecasting with minimal computational time. ADCIRC simulations on the NC9 mesh typically take 60 to 90 minutes during forecasting, depending on the computational resources (Tull 2018). The static method requires 25–35 minutes to run in serial for the large NC DEM (Fig. 2). Each of the three downscaling methods was tested on the smaller Carteret County DEM to compare timing information. The static method was the least computationally costly, requiring 2.23 minutes to complete. The slopes method was the most costly, requiring 13.28 minutes, and the head loss method added minimal cost, requiring 2.76 minutes.

The downscaling methods have a significant effect on the predicted flooding extents. As an example, consider the region near the Newport River (Fig. 11), which includes several small creeks that can convey flows. The native NC9 results (shown in dark blue) show the flooding extends up the river, through a bridge overpass, and over floodplains.

The static method (shown in light blue) tends to over-predict the flood extents (Fig. 11). The flooding is pushed farther into the creeks, such as Deep Creek (point A), which has a low slope and was likely flooded during the storm. In nearly all locations, the flooding extents from the static method are farther inland than the model predictions with the NC9-Carteret mesh. The flooding extents from the slopes method (not shown) are similar. Because the water surface produced by ADCIRC was relatively flat, downscaling using slopes did not differ much compared to the static method. The slopes method can be adjusted using the exaggeration term c from Eq. 1, but inclusion of surface slopes in downscaling ultimately led to minimal change in accuracy with an increased computational cost.

The head loss method (shown in yellow) is the best qualitative match to the true flooding extents. Because the head loss method operates similarly to the static method but uses an energy cost surface (DEM plus head loss) rather than only a DEM, it is impossible for flood extents predicted by the head loss method to exceed those of the static method. However, there are some areas where the head loss method under-predicts flooding. Areas surrounding small rivers were challenging to represent with the head loss method because,

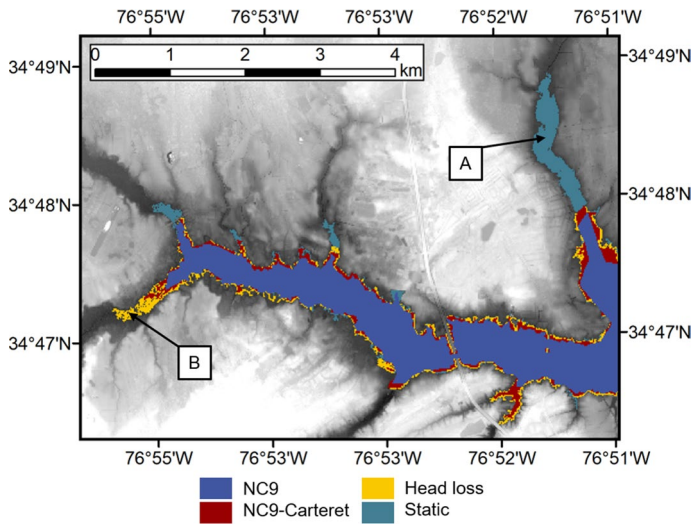


Fig. 11 Example of flooding extents along the Newport River from the ADCIRC models and downscaling methods. Several areas are indicated: **a** represents an area where the head loss method significantly improved the results, compared to the static method and **b** is an area in which the head loss method overestimated flood extents. All rasters shown overlay the DEM used for downscaling. The slopes raster is not shown because the results did not differ enough from the static method

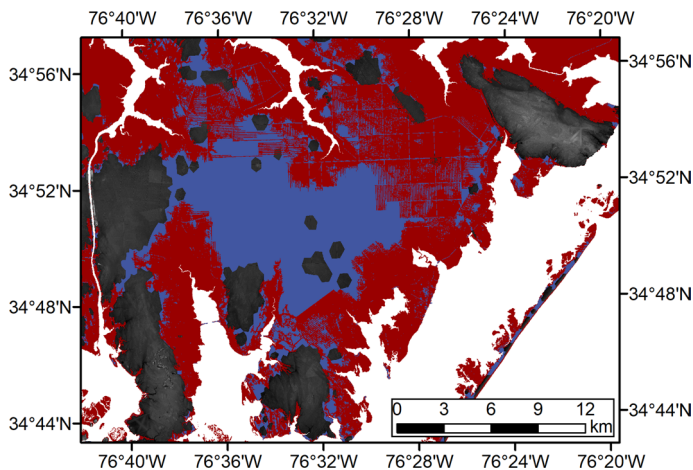


Fig. 12 Example of over-prediction of flooding extents in a simulation on the NC9 mesh. ADCIRC maximum water elevation results from simulations with the NC9 (dark blue) and the NC9-Carteret (red) meshes are shown throughout a low-lying farmland region in eastern Carteret County. The NC9-Carteret results overlay the NC9 results and, for additional context, MSL is shown in white and the DEM is shown in gray scale

during the pre-computational steps where flow paths are traced from MSL, a portion of these rivers were not recognized as perennial bodies of water, due to being narrower than the resolution of the DEM raster. This led to inaccuracies because higher costs were perceived to be required along the river than would have been realistic if the stream had been properly identified. This issue can be fixed by either using a higher-resolution raster or manually delineating perennial water sources.

Another area where the methods performed unfavorably was the low-lying farmland region in eastern Carteret County (Fig. 12). In this region, the simulation using NC9 predicts most of this area to be flooded, while the simulation using the NC9-Carteret mesh does not. The downscaling methods only change the water levels *within* the extents of the NC9 forecast if the DEM exceeds the forecasted water elevation; otherwise, water levels within the extents of the NC9 forecast are considered to be true in downscaling. This leads to a major discrepancy in overall flooded areas between the truth and each downscaling method and shows that the accuracy of the downscaling methods is dependant upon the accuracy of the lower-resolution ADCIRC results. For this reason, the main focus of water level comparisons is outside the extents of the NC9 forecast. The head loss method performs best in areas where the perennial body of water can be easily captured by the raster resolution and the simulation using NC9 does not over-predict flood extents. The Newport River (as shown in Fig. 11) is wide and can be easily delineated automatically without increasing the raster resolution. This allows the head loss method to appropriately calculate accumulation of head loss along flow paths and develop a more accurate cost surface.

Each method was validated quantitatively by comparing different flood extent metrics. The flooding extents from simulations using the NC9 and NC9-Carteret meshes are compared with the downscaled flooding extents from the static, slopes, and head loss methods. The total flooded area, or area of raster cells occupied by water that have an elevation greater than zero (MSL) and are within the study region, is quantified for all five models and methods (Table 2). Next, this same metric is used only for areas outside the extent of NC9. As discussed previously, this is done to remove errors made within the extents of NC9 that are not accounted for in the downscaling methods. The final two metrics compare over- and under-predictions, both outside the extents of NC9. Over-predictions are areas flooded by a downscaling method but not the NC9-Carteret mesh, while under-predictions are areas flooded by the NC9-Carteret mesh but not a downscaling method.

From the flooded areas, it is evident that the performance of each downscaling method is largely dependent upon the performance of the ADCIRC simulation.

Table 2 Comparisons of flooding extents from simulations (using the NC9 and NC9-Carteret meshes) and downscaling methods (static, slopes, and head loss). All values represent flooded areas in km² for Carteret County, NC

Mesh	Downscaling Method	Flooded	Flooded (outside NC9)	Over-Prediction (outside NC9)	Under-Prediction (outside NC9)
NC9	–	636.63	–	–	–
NC9	Static	731.60	98.36	57.56	0.43
NC9	Slopes	707.73	96.46	55.57	0.34
NC9	Head Loss	657.14	52.18	25.12	14.17
NC9-Cart.	–	513.91	41.23	–	–

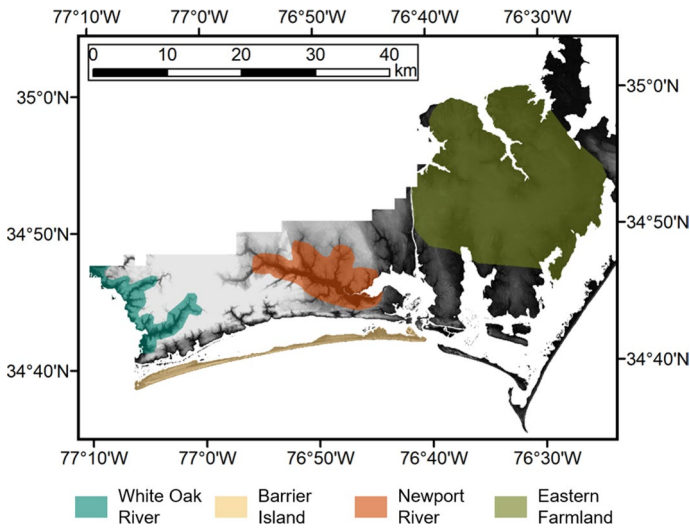


Fig. 13 The four regions used for comparing downscaling method performance are the White Oak River region (blue-green), the barrier island region (tan), the Newport River region (orange), and the eastern farmland region (green)

Due primarily to the topographically low farmland region in eastern Carteret County (Fig. 13), the simulation using the NC9 mesh over-predicted the flooded area with a predicted 636.63 km^2 compared to the NC9-Carteret results of 513.91 km^2 . The static method performed poorest, producing the most flooded area outside NC9 (98.36 km^2). The slopes method performed slightly better with a flooded area of 96.46 km^2 outside NC9, but at a much higher computational cost than the other methods. The head loss method performed best, predicting 52.18 km^2 flooded area outside the extents of NC9 compared to the truth of 41.23 km^2 .

Four regions were analyzed individually (Fig. 13). Each region has different geographical features. The White Oak River region contains a large river system with a large river width and well-defined tributary streams. The Newport River region is still a large river system, but the river is not as wide and its tributary streams are slightly smaller. The barrier island region relies on shorter extrapolation distances but contains more hard structures that create sea walls, canals, and other barriers. Finally, the eastern farmland region has a low topography with a complex system of canals.

The head loss method outperformed the static method in each region (Table 3), with close matches to the true flooded areas. However, the head loss method tends to slightly under-predict flood extents in riverine environments, such as the White Oak River (flooded area outside NC9 of 2.28 km^2 , compared to a true flooded area of 4.29 km^2) and the Newport River (3.81 km^2 , compared to 3.96 km^2). This may be due to the fact that, within smaller tributary stream areas, flood extents generated by ADCIRC extend farther away from MSL than they do in other regions. Therefore, the cost accounted for by ADCIRC output (Fig. 8, panels c and f) is much higher and can lead to inaccuracies as these costs are taken into account in downscaling. These under-predictions can be managed by either manually delineating perennial water sources to reduce the cost accounted for by ADCIRC output or reducing the friction values associated with

Table 3 Regional flooded area (km²) comparisons between the NC9-Carteret mesh simulation results and the head loss and static downscaling method results

Mesh	Barrier Island region		
	Downscaling method	Flooded	Flooded (outside NC9)
NC9	Static	9.16	5.05
NC9	Head Loss	6.95	3.13
NC9-Carteret	–	6.33	3.02
Mesh	Newport river region		
	Downscaling method	Flooded	Flooded (outside NC9)
NC9	Static	22.44	7.08
NC9	Head Loss	19.06	3.81
NC9-Carteret	–	18.89	3.96
Mesh	White Oak river region		
	Downscaling method	Flooded	Flooded (outside NC9)
NC9	Static	9.83	6.47
NC9	Head Loss	5.56	2.28
NC9-Carteret	–	7.51	4.29
Mesh	Eastern farmland region		
	Downscaling method	Flooded	Flooded (outside NC9)
NC9	Static	409.44	34.04
NC9	Head Loss	374.65	19.39
NC9-Carteret	–	248.01	7.32
NC9	–	376.50	135.81 ¹

¹For the eastern farmland region, the area represented is flooded outside the NC9-Carteret results

these tributary stream areas. These under-predictions may also be caused by the lack of a velocity head in the downscaling method. This would be a way to represent the additional momentum in these tributaries, and thus to extend farther the predicted inundation.

6 Conclusions

Accurate, timely predictions of storm surge and flooding are critical to managers in the event of an approaching storm. Predictive models for storm surge and coastal flooding must balance computational time with model resolution. These models are not able to simulate flooding at the finest scales of available DEMs, which can resolve small-scale infrastructure such as roads, buildings, and neighborhoods of interest to emergency managers. This study presents three GIS-based techniques for downscaling (or increasing the resolution of) ADCIRC storm surge predictions in real-time forecasting and validates the results using an ADCIRC simulation with the higher-resolution NC9-Carteret mesh. These techniques can provide emergency managers with accurate forecast results at high resolution in a reasonable time for decision-making during an impending storm event.

The major conclusions of this research are summarized below:

1. *The static method provides results at low computational cost, but over-predicts water level extents.* Outside the extents of the NC9 water elevation forecast for Hurricane Florence (2018), the static method predicted 98.36 km² to be flooded throughout Carteret County, while an ADCIRC simulation on the NC9-Carteret mesh (taken as the truth) predicted 41.23 km² to be flooded. Although the method over-predicts flood extents, it can still provide useful information to emergency managers if a conservative estimation is desired. With a minimal amount of raster operations, the static method is the least costly in computational time.
2. *Downscaling using the slopes method did not improve the downscaling simulations.* The water elevation surface slopes were small, so extrapolating while using these slopes did not affect the downscaled water elevations. In relation to the static method, which produced a flooded area of 98.36 km² outside the extents of the NC9 results, the slopes method flooded 96.46 km². The slopes method also has a significantly higher computational cost compared to the static method; forecasting over large domains would require parallelization. This method is not recommended over either of the other proposed methods.
3. *The head loss method performed best and allows for the most flexibility.* Outside the extent of the NC9 model results, the head loss method had a 52.18 km² flooded area while the NC9-Carteret model had 41.23 km². The head loss method extrapolates water levels to an energy cost surface, consisting of energy head due to changes in elevation, added to head loss due to friction from land cover. Most of the computations for creating the energy cost surface are done prior to receiving input from ADCIRC models, so, because time is not a limiting factor in the pre-computational process, the head loss method allows for the most flexibility.

Further research may involve running series of storm simulations using high-resolution ADCIRC models (or using another source as truth) and tuning parameters to best match the desired results. This can be done using ADCIRC results from both historical storms and synthetic storms. The downscaling methods may also be improved by the use of a velocity head in the head loss method, and thus the inclusion of additional momentum as the flooding is extended into tributaries and active waterways. The accuracy of storm surge simulations will continue to improve, as flooding predictions will continue to be critical to emergency managers for decision-making before, during, and after storms.

The methods presented in this research will provide important tools for emergency managers evaluating storm surge predictions at high resolutions.

Funding This material is based upon work supported by the U.S. Department of Homeland Security under Grant Award Number 2015-ST-061-ND0001-01. The views and conclusions contained herein are those of the authors and should not be interpreted as necessarily representing the official policies, either expressed or implied, of the U.S. Department of Homeland Security. This material is also based upon work supported by the National Science Foundation under Grant Award Number ICER-1664037, and by the National Consortium for Data Science. This work used the Extreme Science and Engineering Discovery Environment (XSEDE), which is supported by National Science Foundation Grant Number ACI-1548562.

Data availability The geospatial datasets are available publicly. DEMs are available from the North Carolina Spatial Data Download (<https://sdd.nc.gov/sdd/>) and the USGS National Geospatial Program (<https://viewer.nationalmap.gov/advanced-viewer/>). Land cover data are available from the Multi-Resolution Land Characteristics Consortium (<https://www.mrlc.gov/viewer/>). ADCIRC forecast data are available from the Coastal Emergency Risks Assessment (<https://cera.coastalrisk.live>).

Declarations

Conflict of interest The authors have no conflict of interest.

Code Availability The downscaling scripts are available publicly from an open-source repository (<https://github.com/ccht-ncsu/Kalpana>) with documentation (<https://ccht.ccee.ncsu.edu/kalpana/>). ADCIRC can be requested via its web site (<http://adcirc.org>).

References

- Aerts JCJH, Lin N, Botzen WJW, Emanuel K, de Moel H (2013) Low-probability flood risk modeling for New York City. *Risk Anal* 33:772–778
- Bates PD, de Roo APJ (2000) A simple raster-based model for flood inundation simulation. *J Hydrol* 236:54–77
- Bates PD, Dawson RJ, Hall JW, Horritt MS, Nicholls RJ, Wicks J, Hassan MAAM (2005) Simplified two-dimensional numerical modelling of coastal flooding and example applications. *Coast Eng* 52:793–810
- Blanton BO, Luettich RA (2008) North Carolina Coastal Flood Analysis System: Model Grid Generation. Technical Report TR-08-05, Renaissance Computing Institute
- Blanton BO, Luettich RA (2010) North Carolina Floodplain Mapping Program, Coastal Flood Insurance Study: Water Level Validation Study. Technical Report TR-10-06, Renaissance Computing Institute
- Blanton BO, Madry S, Gallupi K, Gamiel K, Lander H, Reed M, Stillwell L, Blanchard-Montgomery M, Luettich R, Mattocks C, Fulcher C, Vickery P, Hanson J, Devaliere E, McCormick J (2008) Report for State of North Carolina Floodplain Mapping Project Coastal Flood Analysis System. Technical Report TR-08-08, Renaissance Computing Institute
- Blanton BO, McGee J, Fleming JG, Kaiser C, Kaiser H, Lander H, Luettich RA, Dresback KM, Kolar RL (2012) Urgent computing of storm surge for North Carolina's coast. *Proc Int Conf Comput Sci* 9:1677–1686
- Blumberg AF, Georgas N, Yin L, Herrington TO, Orton PM (2015) Street-scale modeling of storm surge inundation along the New Jersey Hudson River waterfront. *Jo Atmos Ocean Technol* 32:1486–1497
- Booij N, Ris RC, Holthuijsen LH (1999) A third-generation wave model for coastal regions, Part I, Model description and validation. *J Geophys Res* 104:7649–7666
- Brown I (2006) Modelling future landscape change on coastal floodplains using a rule-based GIS. *Environ Model Softw* 21:1479–1490
- Bunya S, Dietrich JC, Westerink JJ, Ebersole BA, Smith JM, Atkinson JH, Jensen RE, Resio DT, Luettich RA, Dawson CN, Cardone VJ, Cox AT, Powell MD, Westerink HJ, Roberts HJ (2010) A high-resolution coupled riverine flow, tide, wind, wind wave and storm surge model for southern Louisiana and Mississippi: Part I - Model development and validation. *Mon Weather Rev* 138:345–377


- Cheung KF, Phadke AC, Wei Y, Rojas R, Douyere YJM, Martino CD, Houston SH, Liu PLF, Lynett PJ, Dodd N, Liao S, Nakazaki E (2003) Modeling of storm-induced coastal flooding for emergency management. *Ocean Eng* 30:1353–1386
- Comer J, Olbert AI, Nash S, Hartnett M (2017) Development of high-resolution multi-scale modelling system for simulation of coastal-fluvial urban flooding. *Nat Hazards Earth Syst Sci* 17:205–224
- Cyriac R, Dietrich JC, Fleming JG, Blanton BO, Kaiser C, Dawson CN, Luettich RA (2018) Variability in coastal flooding predictions due to forecast errors during Hurricane Arthur (2014). *Coast Eng* 137:59–78
- Dietrich JC, Westerink JJ, Kennedy AB, Smith JM, Jensen RE, Zijlema M, Holthuijsen LH, Dawson CN, Luettich RA, Powell MD, Cardone VJ, Cox AT, Stone GW, Pourtaheri H, Hope ME, Tanaka S, Westerink LG, Westerink HJ, Cobell Z (2011a) Hurricane Gustav (2008) waves and storm surge: Hindcast, validation and synoptic analysis in southern Louisiana. *Mon Weather Rev* 139:2488–2522
- Dietrich JC, Zijlema M, Westerink JJ, Holthuijsen LH, Dawson CN, Luettich RA, Jensen RE, Smith JM, Stelling GS, Stone GW (2011) Modeling hurricane waves and storm surge using integrally-coupled, scalable computations. *Coast Eng* 58:45–65
- Dietrich JC, Tanaka S, Westerink JJ, Dawson CN, Luettich RA, Zijlema M, Holthuijsen LH, Smith JM, Westerink LG, Westerink HJ (2012) Performance of the unstructured-mesh, SWAN+ADCIRC model in computing hurricane waves and surge. *J Sci Comput* 52:468–497
- Dietrich JC, Trahan CJ, Howard MT, Fleming JG, Weaver RJ, Tanaka S, Yu L, Luettich RA, Dawson CN, Westerink JJ, Wells G, Lu A, Vega K, Kubach A, Dresback KM, Kolar RL, Kaiser C, Twilley RR (2012) Surface trajectories of oil transport along the northern coastline of the gulf of mexico. *Cont Shelf Res* 41:17–47
- Dietrich JC, Dawson CN, Proft J, Howard MT, Wells G, Fleming JG, Luettich RA, Westerink JJ, Cobell Z, Vitse M (2013) Real-time forecasting and visualization of hurricane waves and storm surge using SWAN+ADCIRC and FigureGen. In Dawson CN, Gerritsen M, editors, *Computational Challenges in the Geosciences*, pp 49–70
- Dietrich JC, Muhammad A, Curcic M, Fathi A, Dawson CN, Chen SS, Luettich RA (2018) Sensitivity of storm surge predictions to atmospheric forcing during Hurricane Isaac. *Journal of Waterway, Port, Coastal and Ocean Engineering*, 144
- Dresback KM, Fleming JG, Blanton BO, Kaiser C, Gourley JJ, Tromble EM, Luettich RA, Kolar RL, Hong Y, Van Cooten S, Vergara HJ, Flamig Z, Lander HM, Kelleher KE, Nemunaitis-Monroe KL (2013) Skill assessment of a real-time forecast system utilizing a coupled hydrologic and coastal hydrodynamic model during Hurricane Irene (2011). *Cont Shelf Res* 71:78–94
- Fleming J, Fulcher C, Luettich RA, Estrade B, Allen G, Winer H (2008) A real time storm surge forecasting system using ADCIRC. *Estuar Coast Model* 2007:893–912
- Forbes C, Luettich RA, Mattocks CA, Westerink JJ (2010) A retrospective evaluation of the storm surge produced by Hurricane Gustav (2008): Forecast and hindcast results. *Wea Forecast* 25:1577–1602
- Fritz HM, Blount C, Sokoloski R, Singleton J, Fuggle A, McAdoo BG, Moore A, Grass C, Tate B (2007) Hurricane Katrina storm surge distribution and field observations on the Mississippi barrier islands. *Estuar Coast Shelf Sci* 74:12–20
- Gallien TW, Schubert JE, Sanders BF (2011) Predicting tidal flooding of urbanized embayments: A modeling framework and data requirements. *Coast Eng* 58:567–577
- Gao J (2018) On the surface wind stress for storm surge modeling. PhD thesis, University of North Carolina at Chapel Hill
- Garratt JR (1977) Review of drag coefficients over oceans and continents. *Mon Weather Rev* 105:915–929
- GRASS Development Team. r.walk. Open Source Geospatial Foundation, 2002. URL <https://grass.osgeo.org/grass78/manuals/r.walk.html>. [Retrieved 08 February 2021]
- GRASS Development Team. Geographic Resources Analysis Support System (GRASS GIS) Software, Version 7.2. Open Source Geospatial Foundation, 2017. URL <http://grass.osgeo.org>
- Hartnett M, Nash S (2017) High-resolution flood modeling of urban areas using MSN_Flood. *Water Sci Eng* 10:175–183
- Heberger M, Cooley H, Herrera P, Gleick PH, Moore E (2009) The impacts of sea-level rise on the California coast. Technical report, California Climate Change Center
- Hope ME, Westerink JJ, Kennedy AB, Kerr PC, Dietrich JC, Dawson CN, Bender CJ, Smith JM, Jensen RE, Zijlema M, Holthuijsen LH, Luettich RA Jr, Powell MD, Cardone VJ, Cox AT, Pourtaheri H, Roberts HJ, Atkinson JH, Tanaka S, Westerink HJ, Westerink LG (2013) Hindcast and Validation of Hurricane Ike (2008) Waves, Forerunner, and Storm Surge. *J Geophys Res Oceans* 118:4424–4460
- Interagency Performance Evaluation Task Force (2008) Performance evaluation of the New Orleans and south-east Louisiana hurricane protection system. Technical report, US Army Corps of Engineers
- Kalyanapu A, Burian S, Mcpherson TN (2009) Effect of land use-based surface roughness on hydrologic model output. *J Spat Hydrol* 9(2):51–71

- Kerr PC, Donahue AS, Westerink JJ, Luettich RA, Zheng LY, Weisburg RH, Huang Y, Wang HV, Teng Y, Forrest DR, Roland A, Haase AT, Kramer AW, Taylor AA, Rhome JR, Feyen JC, Signell RP, Hanson JL, Hope ME, Estes RM, Dominguez RA, Dunbar RP, Semeraro LN, Westerink HJ, Kennedy AB, Smith JM, Powell MD, Cardone VJ, Cox AT (2013) U.S. IOOS coastal and ocean modeling testbed: Inter-model evaluation of tides, waves, and hurricane surge in the Gulf of Mexico. *J Geophys Res Oceans* 118:5129–5172
- Knowles N (2010) Potential inundation due to rising sea levels in the San Francisco Bay region. *San Francisco Estuary and Watershed Science*, 8
- Larson M, Clements G (2008) r.grow. Open Source Geospatial Foundation, URL <https://grass.osgeo.org/grass78/manuals/r.grow.html>
- Lichter M, Felsenstein D (2012) Assessing the costs of sea-level rise and extreme flooding at the local level: A GIS-based approach. *Ocean Coast Manag* 59:47–62
- Liu Z, Merwade V, Jafarzadegan K (2018) Investigating the role of model structure and surface roughness in generating flood inundation extents using one- and two-dimensional hydraulic models. *Flood Risk Manag* 12(1):1–19
- Mayo T, Butler T, Dawson C, Hoteit I (2014) Data assimilation within the Advanced Circulation (ADCIRC) modeling framework for the estimation of Manning's friction coefficient. *Ocean Model* 76:43–58
- Medeiros SC, Hagen SC (2013) Review of wetting and drying algorithms for numerical tidal flow models. *Int J Numer Meth Fluids* 71:473–487
- Mitas L, Mitasova H, Kosinovsky I, McCauley D, Hofierka J, Zubal S, Lacko M v.surf.rst. Open Source Geospatial Foundation. URL <https://grass.osgeo.org/grass79/manuals/v.surf.rst.html>
- Mitasova H, Mitas L, Harmon RS (2005) Simultaneous spline approximation and topographic analysis for lidar elevation data in open-source gis. *IEEE Geosci Remote Sens Lett* 2:375–379
- Multi-Resolution Land Characteristics Consortium. MRLC Viewer, 2019. URL <https://www.mrlc.gov/viewer/>
- Olbert AI, Comer J, Nash S, Hartnett M (2017) High-resolution multi-scale modelling of coastal flooding due to tides, storm surges and rivers inflows: A Cork City example. *Coast Eng* 121:278–296
- Passeri D, Hagen SC, Smar D, Alimohammadi N, Risner A, White R (2011) Sensitivity of an ADCIRC Tide and Storm Surge Model to Manning's n. *Estuar Coast Model* 4(3):457–475
- Poulter B, Halpin PN (2008) Raster modelling of coastal flooding from sea-level rise. *International Journal of Geographic Information Science*, pages 167–182
- Purvis MJ, Bates PD, Hayes CM (2008) A probabilistic methodology to estimate future coastal flood risk due to sea level rise. *Coast Eng* 55:1062–1073
- Ramirez JA, Lichter M, Coulthard TJ, Skinner C (2016) Hyper-resolution mapping of regional storm surge and tide flooding: comparison of static and dynamic models. *Nat Hazards* 82:571–590
- Rubin H, Atkinson J (2001) *Environmental Fluid Mechanics*. Marcel Dekker, 270 Madison Avenue, New York, NY 10016
- Sebastian AG, Proft JM, Dietrich JC, Du W, Bedient PB, Dawson CN (2014) Characterizing hurricane storm surge behavior in Galveston Bay using the SWAN+ADCIRC model. *Coast Eng* 88:171–181
- Shapiro M, Clements G (1991) r.mapcalc. Open Source Geospatial Foundation, URL <https://grass.osgeo.org/grass78/manuals/r.mapcalc.html>
- Shapiro M, Metz G (2008) r.clump. Open Source Geospatial Foundation, URL <https://grass.osgeo.org/grass78/manuals/r.clump.html>
- Smith A, Lott N, Houston T, Shein K, Crouch J, Enloe J (2020) U.S. Billion-Dollar Weather and Climate Disasters 1980–2019. Technical report, NOAA National Centers for Environmental Information (NCEI)
- Stewart SR, Berg R (2019) Tropical Cyclone Report for Hurricane Florence, 31 August - 17 September 2018. Technical report, National Hurricane Center
- Tull N (2018) Improving accuracy of real-time storm surge inundation predictions. Master's thesis, North Carolina State University, Raleigh, NC, USA
- U.S. Geological Survey. Flood event viewer. <https://stn.wim.usgs.gov/FEV/#FlorenceSep2018>, 2020. [Retrieved 16 June 2020]
- Wang HV, Loftis JD, Liu Z, Forrest D, Zhang J (2014) The storm surge and sub-grid inundation modeling in New York City during Hurricane Sandy. *J Mar Sci Eng* 2:226–246
- Westerink JJ, Muccino JC, Luettich RA (1992) Resolution requirements for a tidal model of the Western North Atlantic and Gulf of Mexico. In Russell TF et al editor, *Computational Methods in Water Resources*, pp 669–674
- Westerink JJ, Luettich RA Jr, Feyen JC, Atkinson JH, Dawson CN, Roberts HJ, Powell MD, Dunion JP, Kubatko EJ, Pourtaheri H (2008) A basin to channel scale unstructured grid hurricane storm surge model applied to Southern Louisiana. *Mon Weather Rev* 136:833–864
- Westerveldt J, Shapiro M (2008) r.reclass. Open Source Geospatial Foundation, URL <https://grass.osgeo.org/grass78/manuals/r.reclass.html>

- Yin J, Lin N, Yu D (2016) Coupled modeling of storm surge and coastal inundation: a case study in New York City during Hurricane Sandy. *Water Resour Res* 52:8685–8699
- Yu D, Lane SN (2006) Urban fluvial flood modelling using a two-dimensional diffusion-wave treatment, part 1: Mesh resolution effects. *Hydrol Process* 20:1541–1565
- Zijlema M (2010) Computation of wind-wave spectra in coastal waters with SWAN on unstructured grids. *Coast Eng* 57:267–277

Publisher's Note Springer Nature remains neutral with regard to jurisdictional claims in published maps and institutional affiliations.

Authors and Affiliations

C. A. Rucker^{1,2} · N. Tull^{1,3} · J. C. Dietrich¹  · T. E. Langan⁴ · H. Mitasova⁵ · B. O. Blanton⁶ · J. G. Fleming⁷ · R. A. Luettich Jr⁸

C. A. Rucker
carucker@ncsu.edu

N. Tull
ntull@ncsu.edu

T. E. Langan
tom.langan@ncdps.gov

H. Mitasova
hmitaso@ncsu.edu

B. O. Blanton
bblanton@renci.org

J. G. Fleming
jason.fleming@seahorsecoastal.com

R. A. Luettich Jr
rick_luettich@unc.edu

¹ Dep't of Civil, Construction, and Environmental Engineering, North Carolina State University, Raleigh, NC, USA

² Present Address: U.S. Army Corps of Engineers, Wilmington District, Wilmington, NC, USA

³ Present Address: University of Texas at Austin, Austin, TX, USA

⁴ North Carolina Floodplain Mapping Program, NC Emergency Management, Raleigh, NC, USA

⁵ Center for Geospatial Analytics, North Carolina State University, Raleigh, NC, USA

⁶ Renaissance Computing Institute, University of North Carolina at Chapel Hill, Chapel Hill, NC, USA

⁷ Seahorse Coastal Consulting, Morehead City, NC, USA

⁸ Institute of Marine Science, University of North Carolina at Chapel Hill, Morehead City, NC, USA